A 3-D Boundary Element Method for Dynamic Analysis of Anisotropic Elastic Solids[1]

M. Kögl, L. Gaul[2]

Abstract: A Boundary Element formulation is presented for the solution of three-dimensional problems of anisotropic elastodynamics. Due to the complexity of the dynamic fundamental solutions for anisotropic materials and the resulting high computational costs, the approach at hand uses the fundamental solution of the static operator. This leads to a domain integral in the representation formula which contains the inertia term. The domain integral can be transformed to the boundary using the Dual Reciprocity Method. This results in a system of ordinary differential equations in time with time-independent matrices. Several general questions concerning the anisotropic solutions, the use of DRM, and the choice of the time stepping scheme are investigated by numerical examples, and the capacity of the method for the solution of forced vibration problems and transient analyses is demonstrated. The results show excellent agreement for the displacements, and an improved accuracy in stress calculations when compared to Finite Element analyses.

keyword: anisotropy, boundary element method, dual reciprocity method, dynamic analysis, fundamental solution, particular solution

1 Introduction

Growing requirements of modern engineering structures necessitate the development and use of new materials. An increasing number of these materials is anisotropic, among others composite materials, which have gained importance in a wide range of applications, as e.g. in aero- and astronautics. This raises the demand for numerical techniques which can accurately account for material anisotropy. In the past two decades, Boundary Element Methods have emerged as a very powerful tool for the numerical computation of problems of mathematical physics. Their most striking feature is the fact that only the boundary of the domain needs to be discretized, rather than the domain itself. This offers significant advantages over other discretization methods such as the Finite Element Method. Depending on the complexity of the actual structure and load case under investigation, this simplified discretization can lead to important time savings in the mesh creation and modification process. Therefore, extensive research activities on Boundary Element Methods have been undertaken, and their range of applicability has been extended to many areas of engineering such as structural mechanics, fluid dynamics, heat transfer, electromagnetics, etc.

In general, Boundary Element Methods are very well suited for mechanical problems, especially for problems involving infinite or semi-infinite domains (acoustics, soil-structure interaction, etc.) and for stress concentration problems. This is because they make use of the so-called fundamental solution, which is an analytical free space solution of the governing differential equations for point source excitation, and thus represents far-fields and stresses very accurately. However, it is this very fundamental solution which, albeit being responsible for the advantages of the Boundary Element Methods, also poses some problems in anisotropic analyses with Boundary Elements. Due to the complexity of the anisotropic field equations, closed form fundamental solutions for three-dimensional anisotropic elasticity only exist for special cases like transversely isotropic or cubic media (see e.g. Dederichs and Leibfried (1969); Pan and Chou (1976); Ding, Liang, and Chen (1997)). For general anisotropic elastostatics, for which the elasticity tensor contains up to 21 independent material constants, only an integral representation as given, e.g., by Bacon, Barnett, and Scattergood (1980) is available. The computation of this fundamental solution is extremely time consuming, so that it should not be used directly in a BE program code. However, the integral depends only on two coordinates. This allows pre-computation and storage in a two-dimensional array, so that the fundamental solution can rapidly be evaluated in the actual BE program by interpolation from this array. Therefore, the lack of a closed form fundamental solution should not be considered as a drawback in elastostatics. Among others, Vogel and Rizzo (1973); Wilson and Cruse (1978); Deb (1991); Schclar (1994) have obtained good results using anisotropic Boundary Element formulations.

The situation is different for three-dimensional elastodynamics. In the frequency- as well as in the time-domain, integral expressions for the fundamental solutions have been derived recently by Wang and Achenbach (1993, 1994, 1995) using the Radon transform. Unfortunately, the interpolation approach used for the static fundamental solution cannot be applied here, for reasons that will be explained later. Since the computational costs for the evaluation of the dynamic fundamental solutions are even higher than for the static solution, their use in a Boundary Element code does not seem to be

[1] Dedicated to Professor Dietmar Gross on the occasion of his 60th birthday

[2] Institute A of Mechanics, University of Stuttgart, Germany

very promising. It is probably due to these problems that, to the best of the authors' knowledge, no implementation of a direct Boundary Element Method for three-dimensional problems of anisotropic elastodynamics can be found in the literature. However, it should be noted that anisotropic wave scattering problems have been solved successfully in two dimensions by Wang, Achenbach, and Hirose (1996), and in three dimensions using an indirect BEM by Zheng and Dravinski (2000).

The aim of the present article is therefore to close this gap and present a Boundary Element Method which allows an accurate calculation of anisotropic elastodynamics. Since the implementation of the anisotropic static fundamental solution does not present any important obstacles, contrary to the anisotropic dynamic fundamental solutions, it is the authors' opinion that a practical Boundary Element formulation of elastodynamics should employ the static fundamental solution.

When using the static fundamental solution in the Boundary Element formulation, an additional domain integral, which contains the effects of inertia, appears in the representation formula. In order to avoid the discretization of the domain, which would greatly reduce the attractiveness of the Boundary Element Method, this domain integral has to be transformed to the boundary. This can be done very elegantly by using the Dual Reciprocity Method (DRM), proposed by Nardini and Brebbia (1982) for free vibration analysis in isotropic elasticity. The Dual Reciprocity approach leads to a system of equations with time independent mass and stiffness matrices, similar to the systems known from elastic Finite Element analysis. Apart from avoiding the use of the anisotropic dynamic fundamental solution, several other advantages result from this formulation, concerning the calculation of free vibrations and transient analyses (see e.g. Nardini and Brebbia (1985, 1986)).

The present article first introduces the basics of anisotropic analysis using Boundary Elements, considering the derivation of the Dual Reciprocity equations, representation formula, and the process leading to the final system of equations. After that, the anisotropic fundamental and particular solutions and their implementation are discussed. Finally, some general questions arising in anisotropic BE analysis are investigated, and a number of three-dimensional example problems are solved.

2 Basic equations

The basic equations governing the motion of an elastic body in the linear theory of elasticity are the balance of momentum and moment of momentum, respectively

$$\sigma_{ij,j} + b_i = \rho \ddot{u}_i \,, \qquad \sigma_{ij} = \sigma_{ji} \,, \tag{1}$$

which describe the dynamics of an elastic body. The infinitesimal strain tensor

$$\varepsilon_{kl} = \frac{1}{2}\left(u_{k,l} + u_{l,k}\right) \tag{2}$$

describes the kinematics of deformation, and Hooke's law for an anisotropic body

$$\sigma_{ij} = C_{ijkl}\varepsilon_{kl} \tag{3}$$

connects the kinematic and kinetic variables. The physical quantities introduced in Eqs. 1-3 are the Cauchy stress tensor σ_{ij}, body force density b_i, displacements u_i, strain tensor ε_{kl}, mass density ρ, and elasticity tensor C_{ijkl}. Here and in the following, Einstein's summation convention is applied, the comma denotes partial differentiation with respect to the spatial coordinates, and the superimposed dot denotes partial differentiation with respect to time. The material tensor exhibits the symmetries

$$C_{ijkl} = C_{jikl} = C_{klij} \,, \tag{4}$$

thus for general anisotropy it contains up to 21 independent material constants. The traction vector t_i is related to the displacement vector u_k through Cauchy's formula $t_i = \sigma_{ij} n_j$, which leads to

$$t_i = C_{ijkl} u_{k,l} n_j \,, \tag{5}$$

where n_j denotes a unit vector pointing in the direction in which the traction vector is evaluated.

Now, introducing the elliptic operator of anisotropic elastostatics

$$L_{ik} := C_{ijkl}\partial_l \partial_j \,, \tag{6}$$

the motion of an anisotropic elastic body can be described by Navier's equations

$$L_{ik} u_k + b_i = \rho \ddot{u}_i \,, \tag{7}$$

which can be obtained from Eqs. 1-3, and suitable boundary conditions

$$u_i = \overline{u}_i \quad \text{on } \Gamma_u \,, \tag{8}$$

$$t_i = \overline{t}_i \quad \text{on } \Gamma_t \,, \tag{9}$$

where the bar denotes prescribed values, as well as initial conditions

$$u_i(t=0) = u_i^0 \,, \tag{10}$$

$$\dot{u}_i(t=0) = \dot{u}_i^0 \,. \tag{11}$$

3 Dual Reciprocity Boundary Element formulation

To obtain the boundary integral equation (BIE), which is the starting point for the discretization with boundary elements, the representation formulae for the displacement and displacement gradient fields have to be derived first. In this work, the fundamental solution of the anisotropic *static* operator is used instead of the fundamental solution of the dynamic operator, for the reasons already mentioned.

First, Navier's equation (7) is weighted with the fundamental solution, which serves as test function in a weighted residual statement. Because of the use of the static fundamental solution, the representation formula contains a domain integral with inertia and body force terms. This domain integral is transformed to the boundary using the Dual Reciprocity Method, which was first proposed by Nardini and Brebbia (1982) for free vibration analysis in linear isotropic elasticity. As was shown by Polyzos, Dassios, and Beskos (1994), the DRM is equivalent to the particular integrals method, introduced by Ahmad and Banerjee (1986).

3.1 Representation formula

The process of deriving the representation formula for the displacement field is well known from the standard boundary element literature (see e.g. Brebbia, Telles, and Wrobel (1984), Banerjee (1994), Gaul and Fiedler (1996)) and is therefore only briefly outlined here. Weighting Navier's equation (7) with a test function u^*_{mi} and integrating twice by parts, one obtains the reciprocity relation

$$\int_\Omega \left(L_{ik}u_k u^*_{mi} - L_{ik}u^*_{mk}u_i\right)\,\mathrm{d}\Omega = \int_\Gamma \left(u^*_{mi}t_i - t^*_{mi}u_i\right)\,\mathrm{d}\Gamma\,, \tag{12}$$

where $t^*_{mi} := C_{ijkl}u^*_{mk,l}n_j$. Choosing the test function as a fundamental solution of the elastostatic operator

$$L_{ik}u^*_{mk}(x,\xi) = -\delta_{im}\delta(x,\xi) \tag{13}$$

leads to the representation formula

$$u_m(\xi) = \int_\Gamma \left(u^*_{mi}t_i - t^*_{mi}u_i\right)\,\mathrm{d}\Gamma - \int_\Omega u^*_{mi}\left(\rho\ddot{u}_i - b_i\right)\,\mathrm{d}\Omega\,, \tag{14}$$

where the sifting property of the Dirac distribution for $\xi \in \Omega$ has been used.

3.2 Dual Reciprocity formulation

Due to the existence of a domain integral containing the body forces b_i and inertia term $\rho\ddot{u}_i$, Eq. 14 is not a pure boundary representation of the displacement field u_m. However, by using the DRM, it is possible to transform the domain integral to the boundary. To this end a 'dual reciprocity' similar to Eq. 12 is derived by weighting the inhomogeneous differential equation

$$L_{ik}u^q_{kn} = f^q_{in} \tag{15}$$

with the fundamental solution u^*_{mi}. This leads to a 'dual representation formula'

$$u^q_{mn}(\xi) = \int_\Gamma \left(u^*_{mi}t^q_{in} - t^*_{mi}u^q_{in}\right)\mathrm{d}\Gamma - \int_\Omega u^*_{mi}f^q_{in}\,\mathrm{d}\Omega\,. \tag{16}$$

Here, u^q_{kn} is a particular solution of the elastostatic Eq. 15, and $t^q_{in} := C_{ijkl}u^q_{kn,l}n_j$ is the corresponding traction field.

Now the source term in Eq. 14 is approximated by a series of tensor functions f^q_{in} and unknown coefficients α^q_n

$$\rho\ddot{u}_i(x) - b_i(x) \approx \sum_{q=1}^{N} f^q_{in}(x)\,\alpha^q_n\,, \tag{17}$$

so that, by substituting the approximation Eq. 17 into Eq. 14, and making use of Eq. 16, a new representation formula for the displacement field u_k can be obtained

$$u_k(\xi) = \int_\Gamma \left(u^*_{ki}t_i - t^*_{ki}u_i\right)\mathrm{d}\Gamma + \sum_{q=1}^{N}\left(u^q_{kn}(\xi) - \int_\Gamma \left(u^*_{ki}t^q_{in} - t^*_{ki}u^q_{in}\right)\mathrm{d}\Gamma\right)\alpha^q_n\,, \tag{18}$$

representing $u_k(\xi)\ ,\ \xi \in \Omega$ in terms of field quantities on the boundary only. From Eq. 18, the interior displacements $u_k(\xi)$ can be calculated at any point $\xi \in \Omega$ if the boundary solution and the coefficients α^q_n are known.

In order to calculate internal strains and stresses, Eq. 18 has to be differentiated with respect to ξ_l. Taking into account that $\partial/\partial\xi_l = -\partial/\partial x_l$, one obtains

$$\frac{\partial u_k(\xi)}{\partial\xi_l} = -\int_\Gamma \left(u^*_{ki,l}t_i - t^*_{ki,l}u_i\right)\mathrm{d}\Gamma + \sum_{q=1}^{N}\left(\frac{\partial u^q_{kn}(\xi)}{\partial\xi_l} - \int_\Gamma \left(t^*_{ki,l}u^q_{in} - u^*_{ki,l}t^q_{in}\right)\mathrm{d}\Gamma\right)\alpha^q_n\,. \tag{19}$$

It has to be noted that the comma denotes partial differentiation with respect to x, not ξ.

Having calculated the displacement gradient $u_{k,l}$ from Eq. 19, the strains ε_{kl} and stresses σ_{ij} can easily be obtained from Eq. 2 and Eq. 3, respectively.

3.3 Boundary integral equation and discretization

For the solution of a given initial-boundary-value problem, the representation formula Eq. 18 must first be converted into a boundary integral equation (BIE) containing only unknowns on the boundary Γ. Following the well-known procedure of transferring the load point ξ to the boundary and performing the limiting process, one obtains

$$c_{ki}(\xi)u_i(\xi) + \cancel{\int_\Gamma}\, t^*_{ki}u_i\,\mathrm{d}\Gamma - \int_\Gamma u^*_{ki}t_i\,\mathrm{d}\Gamma = \sum_{q=1}^{N}\left(c_{ki}(\xi)u^q_{in}(\xi) + \cancel{\int_\Gamma}\, t^*_{ki}u^q_{in}\,\mathrm{d}\Gamma - \int_\Gamma u^*_{ki}t^q_{in}\,\mathrm{d}\Gamma\right)\alpha^q_n\,, \tag{20}$$

where $\cancel{\int}$ denotes a Cauchy principle value integral, and $c_{ki}(\xi)$ is the free term coefficient at $\xi \in \Gamma$.

The BIE Eq. 20 is now amenable for numerical implementation by the BEM. To this end, the boundary Γ is subdivided into finite surface elements $\Gamma^{(e)}$, which are mapped onto reference elements by means of shape functions and nodal coordinates. In most analyses, the isoparametric concept is used, which means that the same shape functions are also used for the approximation of the displacement and traction fields u_i, t_i, and particular solutions u^q_{in}, t^q_{in}, i.e.,

$$\{x_i, u_i, t_i, u^q_{in}, t^q_{in}\}^{(e)} \approx \sum_m \Phi^m \{\check{x}_i, \check{u}_i, \check{t}_i, \check{u}^q_{in}, \check{t}^q_{in}\}^m , \tag{21}$$

where $\check{(\cdot)}$ denotes nodal values.

Point collocation of the BIE Eq. 20 on the boundary nodes of the discretization yields a system of equations

$$\boldsymbol{H}\check{\boldsymbol{u}} - \boldsymbol{G}\check{\boldsymbol{t}} = \left(\boldsymbol{H}\check{\boldsymbol{U}} - \boldsymbol{G}\check{\boldsymbol{T}}\right)\boldsymbol{\alpha} \tag{22}$$

for the unknown nodal values of the displacement field $\check{\boldsymbol{u}}$ and traction field $\check{\boldsymbol{t}}$. In Eq. 22 the matrices $\check{\boldsymbol{U}}$ and $\check{\boldsymbol{T}}$ stem from the DR formulation and contain the particular solutions. The vector $\boldsymbol{\alpha}$ contains the unknown coefficients from the approximation given in Eq. 17 and can be expressed in terms of nodal values of the body force and acceleration field as described in the next section.

3.4 System of equations

Forcing the approximating series in Eq. 17 to coincide with the source term $\rho\ddot{u}_i - b_i$ at the N collocation points ξ^p of the boundary discretization,

$$\rho\ddot{u}_i(\xi^p) - b_i(\xi^p) = \sum_{q=1}^{N} f^q_{ik}(\xi^p)\,\alpha^q_k , \qquad p = 1 \ldots N \tag{23}$$

leads to a linear system of equations $\rho\check{\ddot{\boldsymbol{u}}} - \check{\boldsymbol{b}} = \boldsymbol{F}\boldsymbol{\alpha}$, the solution of which yields the unknown coefficients

$$\boldsymbol{\alpha} = \boldsymbol{F}^{-1}\left(\rho\check{\ddot{\boldsymbol{u}}} - \check{\boldsymbol{b}}\right) . \tag{24}$$

Replacing the coefficient vector $\boldsymbol{\alpha}$ in Eq. 22 by Eq. 24, one obtains the following system of ordinary differential equations

$$\boldsymbol{M}\check{\ddot{\boldsymbol{u}}} + \boldsymbol{H}\check{\boldsymbol{u}} = \boldsymbol{G}\check{\boldsymbol{t}} + \boldsymbol{V}\check{\boldsymbol{b}} , \tag{25}$$

where the spatial discretization has been performed using a Dual Reciprocity Boundary Element formulation. The volume matrix $\boldsymbol{V}$ and mass matrix $\boldsymbol{M}$ introduced in Eq. 25 are defined by

$$\boldsymbol{V} := \left(\boldsymbol{G}\check{\boldsymbol{T}} - \boldsymbol{H}\check{\boldsymbol{U}}\right)\boldsymbol{F}^{-1} \qquad \text{and} \qquad \boldsymbol{M} := \rho\,\boldsymbol{V} , \tag{26}$$

respectively.

The system of equations in Eq. 25 is similar to the one obtained in Finite Element analysis. Hence solving dynamic problems like transient analysis, free and forced vibrations, can be done in a similar manner. When compared to FE-matrices, the system matrices in the DR-BEM have the disadvantage of being non-symmetric and non-banded. However, due to the reduction of the problem to the boundary, they are much smaller in size than comparable Finite Element matrices.

3.5 About the use of internal nodes

The domain term $\rho\ddot{u}_i - b_i$ is approximated by the series given in Eq. 17. When choosing the interpolation functions f^q_{in} so that the series converges, then an increased number of collocation points will improve the accuracy of the approximation. While it is possible to obtain reasonable results using collocation points on the boundary only, the results improve if a certain number of collocation points are distributed throughout the domain. For some configurations, these internal nodes are even necessary to obtain any results at all. This can be seen by considering a body which is clamped on the whole boundary. If only boundary nodes are used, the complete displacement vector $\boldsymbol{u}$—and hence the acceleration vector $\ddot{\boldsymbol{u}}$—vanishes, so that inertia effects are no longer taken into account. However, by using internal nodes, new degrees of freedom for the displacements are introduced, and inertia effects can be modeled even when the whole boundary is clamped.

4 Fundamental and particular solutions

4.1 Fundamental solutions

The fundamental solution u^*_{mk} of the elastostatic operator L_{ik} is defined by Eq. 13. Due to the complexity of the constitutive tensor C_{ijkl}, closed form solutions for general anisotropy do not exist. However, an integral representation of the fundamental solution can easily be obtained by using the Radon transform, which is described in Gel'fand, Graev, and Vilenkin (1966).

Introducing the tensor function

$$M^{ab}_{mk} = C_{imkl}\,a_i\,b_l \tag{27}$$

where a_i, b_l are arbitrary vectors, the fundamental solution is given by

$$u^*_{mk} = \frac{1}{8\pi^2 r}\oint_0^{2\pi} \left(M^{zz}_{mk}\right)^{-1}\left(z(\phi)\right)\,\mathrm{d}\phi . \tag{28}$$

The contour integration in Eq. 28 has to be performed numerically along a unit circle lying in the plane $z_i r^{\mathrm{o}}_i = 0$, with normal vector r^{o}_i and its centre at the origin (for more details see Bacon, Barnett, and Scattergood (1980)). Since the kernel is regular and well behaved, Gauss quadrature formulae can be used for the numerical integration.

In order to calculate the traction fundamental solutions t^*_{mj} and $t^*_{mj,s}$, the first and second derivatives of u^*_{mk} are needed. They

have been calculated by Barnett (1972) and can also be represented by line integrals along a unit circle

$$u^*_{mk,l} = \frac{1}{8\pi^2 r^2} \oint_0^{2\pi} \left(-r_l^{\mathrm{o}} \left(M^{zz}_{mk}\right)^{-1} + z_l F_{mk} \right) \mathrm{d}\phi \,, \tag{29}$$

$$u^*_{mk,ls} = \frac{1}{8\pi^2 r^3} \oint_0^{2\pi} \Big(2 r_l^{\mathrm{o}} r_s^{\mathrm{o}} \left(M^{zz}_{mk}\right)^{-1} - 2\left(z_l r_s^{\mathrm{o}} + z_s r_l^{\mathrm{o}}\right) F_{mk} + z_l z_s E_{mk} \Big) \mathrm{d}\phi \,, \tag{30}$$

with

$$D_{nq} = M^{r^{\mathrm{o}} z}_{nq} + M^{z r^{\mathrm{o}}}_{nq} \,, \tag{31}$$

$$F_{mk} = \left(M^{zz}_{mn}\right)^{-1} D_{nq} \left(M^{zz}_{qk}\right)^{-1} \,, \tag{32}$$

$$E_{mk} = F_{mn} D_{nq} \left(M^{zz}_{qk}\right)^{-1} + \left(M^{zz}_{mn}\right)^{-1} D_{nq} F_{qk} - 2 \left(M^{zz}_{mn}\right)^{-1} M^{r^{\mathrm{o}} r^{\mathrm{o}}}_{nq} \left(M^{zz}_{qk}\right)^{-1} \,. \tag{33}$$

Now, the traction and traction gradient

$$t^*_{mi} = C_{ijkl} u^*_{mk,l} n_j \,, \tag{34}$$

$$t^*_{mi,s} = C_{ijkl} u^*_{mk,ls} n_j \,, \tag{35}$$

needed in Eq. 18 and Eq. 19, respectively, can be calculated using the derivatives given by Eq. 29 and Eq. 30.

The fundamental solutions in Eqs. 28, 29, and 30 are functions of the distance vector $\vec{r} = \vec{x} - \vec{\xi}$ between the field point $\vec{x}$ and the load point $\vec{\xi}$. They can be written in the following form

$$u^*_{mk} = \frac{1}{r} G^0_{mk}(\theta_1, \theta_2) \,, \tag{36}$$

$$u^*_{mk,l} = \frac{1}{r^2} G^1_{mkl}(\theta_1, \theta_2) \,, \tag{37}$$

$$u^*_{mk,ls} = \frac{1}{r^3} G^2_{mkls}(\theta_1, \theta_2) \,, \tag{38}$$

where the regular functions G^0_{mk}, G^1_{mkl}, and G^2_{mkls} depend only on the polar and azimuth angles $\theta_1 \in [0, \pi]$ and $\theta_2 \in [0, 2\pi]$ of the radius vector $\vec{r} = \vec{r}(r, \theta_1, \theta_2)$, but not on its norm r. Setting up a two-dimensional grid over the angles θ_1 and θ_2 and storing the values of the functions G^0_{mk}, G^1_{mkl}, and G^2_{mkls} for a particular anisotropic material in a corresponding array, it is possible to obtain any value of these functions for arbitrary θ_1 and θ_2 by interpolation from the values stored in the array. Using Eqs. 36-38, the fundamental solutions u^*_{mk}, t^*_{mi} and their derivatives $u^*_{mk,l}$, $t^*_{mi,s}$ which are needed in the implementation can easily be calculated. This procedure greatly speeds up the calculation of the BEM matrices, since the direct evaluation of Eqs. 28-30 is extremely time consuming. As the grid size certainly has an influence on the accuracy of the results, its effect will be the subject of investigation in a later section.

4.2 About the use of the frequency domain fundamental solution

A frequency domain fundamental solution for anisotropic dynamic elasticity has been derived by Wang and Achenbach (1995). It can be written as

$$u^*_{mk} = u^{*,\mathrm{stat}}_{mk} + u^{*,\mathrm{dyn}}_{mk} \,, \tag{39}$$

where the singular static part $u^{*,\mathrm{stat}}_{mk}$ is given by Eq. 28, and the regular dynamic part can be expressed in terms of an integral over half a unit sphere

$$u^{*,\mathrm{dyn}}_{mk}(\vec{r}, \omega) = \frac{\mathrm{i}}{4\pi^2} \int_{\substack{|\vec{n}|=1 \\ \vec{n}\cdot\vec{r}>0}} \sum_{q=1}^{3} \frac{k_{(q)} E_{m(q)} E_{k(q)}}{2\rho c^2_{(q)}} \mathrm{e}^{\mathrm{i} k_{(q)} |\vec{n}\cdot\vec{r}|} \, dS(\vec{n}) \,. \tag{40}$$

In Eq. 40, $\lambda_{(q)}$ and $E_{k(q)}$ are the eigenvalues and corresponding eigenvectors of the Christoffel matrix $\Gamma_{ik}(n) = C_{ijkl} n_j n_l$, which is well known from anisotropic wave propagation theory; $c_{(q)} := \sqrt{\lambda_{(q)}/\rho}$ are the wave velocities of a plane wave, moving in the n-direction, and $k_{(q)} = \omega / c_{(q)}$ are the corresponding wave numbers.

Regarding the regular dynamic part given by Eq. 40, one recognizes that both the angular frequency ω and the radius r appear under the integral. Above all the occurrence of the radius r poses great problems, since it means that the integral now depends on three variables r, θ_1, and θ_2. Consequently, the interpolation array would have to be three-dimensional, with r ranging from 0 to ∞. The same is true for the time-domain fundamental solution of Wang and Achenbach (1993).

The interpolation procedure used for the static fundamental solution can therefore not be used for the dynamic fundamental solutions. Since their direct evaluation, too, is far too time consuming, and because of the advantages of the Dual Reciprocity formulation with respect to the treatment of free vibrations and transient analysis, the authors consider the DRM approach presented in this paper to be the most promising for Boundary Element calculations of anisotropic elasticity problems.

4.3 Particular solutions

As in the case of the fundamental solutions, the complexity of the constitutive tensor prevents the existence of closed form particular solutions. Several methods for an approximate calculation of particular solutions have been presented in the literature, see e.g. Atkinson (1985); Gründemann (1989); Golberg (1995). A much simpler approach, however, has been suggested by Schclar (1994). Instead of choosing radial basis functions for the approximation functions ($f^q_{in} = f^q_{in}(r^q)$) and solving the differential equation 15 to obtain the particular solutions, simply choose $u^q_{kn} = u^q_{kn}(r^q)$ and calculate the

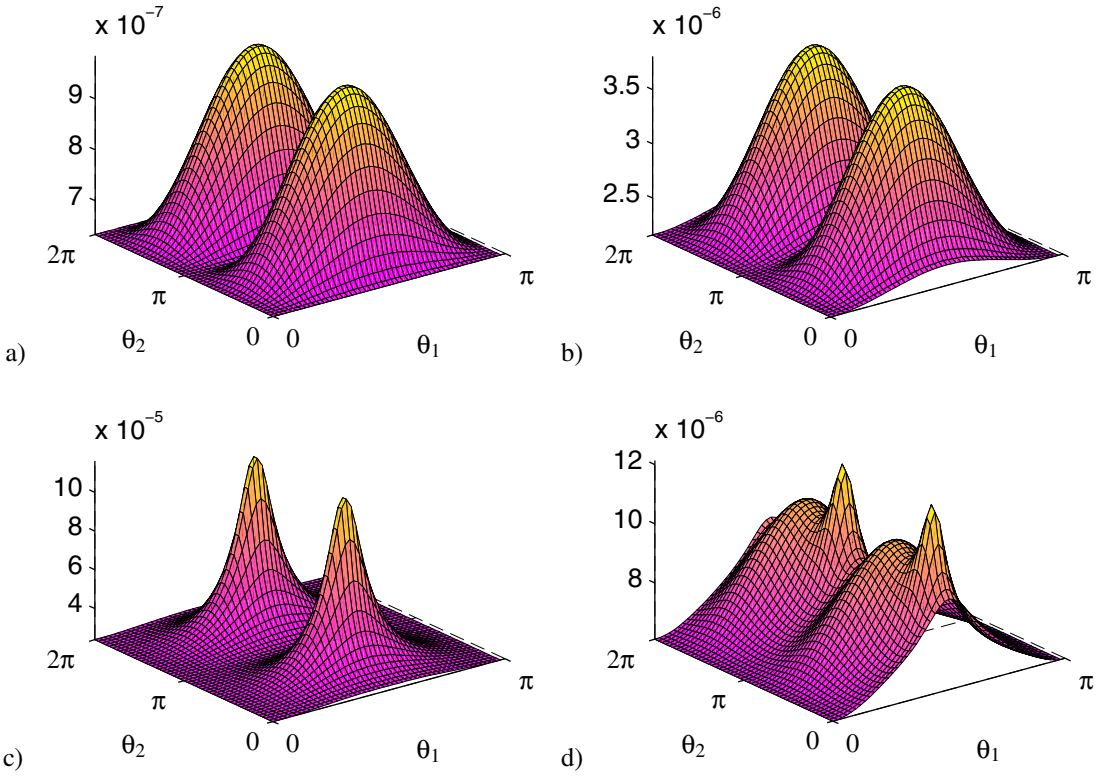

Figure 1 : Fundamental solution ru^*_{22} for: a) steel; b) PIC 151; c) spruce; d) graphite-epoxy

corresponding traction field $t^q_{in} = C_{ijkl}u^q_{kn,l}n_j$ and forcing term $f^q_{in} = C_{ijkl}u^q_{kn,lj}$ by derivation.

This approach is used in the present paper, where the particular solution is chosen as

$$u^q_{kn} = \delta_{kn}\left(r^2 + r^3\right) , \tag{41}$$

which yields the derivatives

$$u^q_{kn,l} = \delta_{kn}(2r + 3r^2)\, r_{,l} , \tag{42}$$

$$u^q_{kn,lj} = \delta_{kn}\left((2+3r)\delta_{lj} + 3r r_{,j} r_{,l}\right) . \tag{43}$$

It is very difficult to make any statements about the convergence of the resulting approximation functions

$$f^q_{in} = C_{ijkl}u^q_{kn,lj} . \tag{44}$$

However, in the present paper, excellent results have been obtained using Eqs. 41-43, as will be shown in the next sections. The question is therefore not addressed any further, but certainly merits to be investigated.

5 General aspects concerning the anisotropic BEM implementation

In the preceding sections, a Boundary Element Method for three-dimensional anisotropic elastodynamics has been developed. Before applying the method to dynamic anisotropic problems, some general questions have to be answered, concerning

- the grid size needed for an accurate interpolation of the fundamental solutions,
- the particular solution used in the interpolation of the domain field, and
- the influence of the internal nodes on the results.

In the following section, calculations for simple elastostatic problems are performed using different materials, in order to determine the influence of the aforementioned aspects on the accuracy of the results.

5.1 Materials

Four materials with different degrees of anisotropy are used in the calculations. Their classification and mass density are

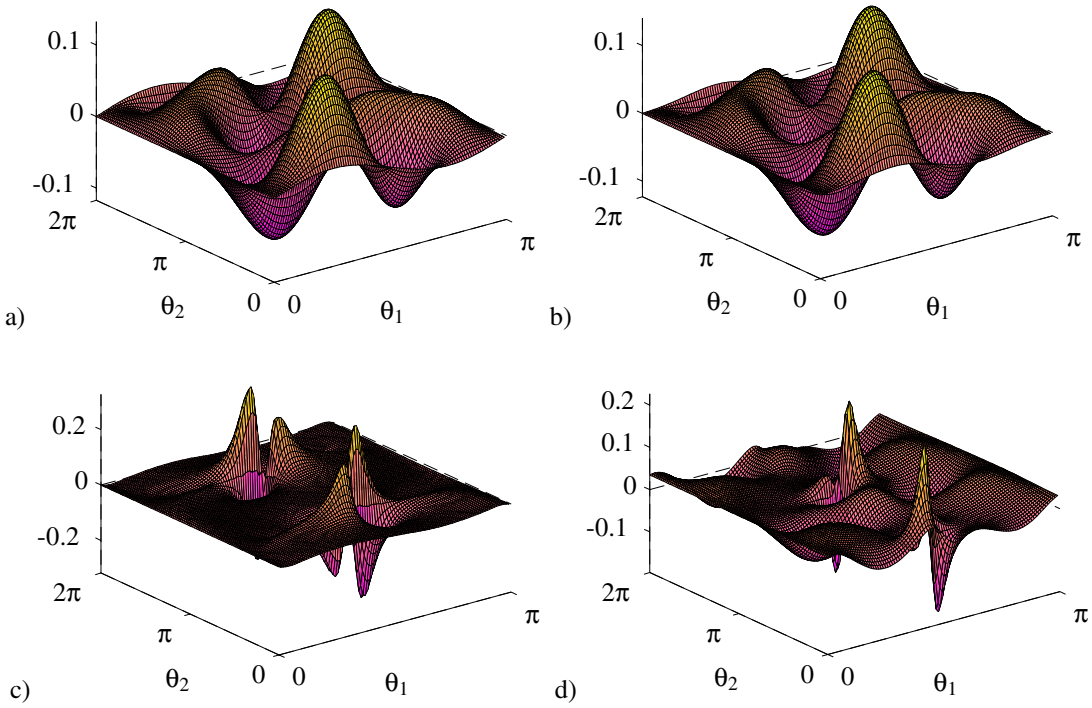

Figure 2 : Fundamental solution $r^3 t^*_{23,1}$ for: a) steel; b) PIC 151; c) spruce; d) graphite-epoxy

given in Tab. 1, the elastic constants can be found in Tab. 2.

5.2 Anisotropic fundamental solution

As mentioned previously, closed form fundamental solutions are known only for certain material classes with a limited number of elastic constants (isotropic, cubic, transversely isotropic). However, since it is the aim of this paper to present a Boundary Element Method applicable to materials with arbitrary degree of anisotropy, the fundamental solution of the general anisotropic elastostatic operator is used, which incorporates all simpler classes such as isotropy and transverse isotropy. This fundamental solution and its derivatives are given by the contour integral representations in Eqs. 28-30.

The integrals over the boundary elements are evaluated numerically, usually by means of Gauss quadrature. This means that the fundamental solution, which appears in the integration kernels, has to be calculated at every Gauss point. The number of Gaussian integration points, however, can be very high, owing to the occurrence of quasi-singular, weakly or strongly singular integrals. Especially for three-dimensional calculations, the computation time needed for the evaluation of the fundamental solutions is a crucial factor in the system matrix calculation. Since the anisotropic fundamental solution does not exist in closed form, the contour integrals have to be evaluated numerically by Gauss quadrature. This is a very time consuming procedure, and doing this at every integration point is much too costly for implementation in a Boundary Element program.

Table 1 : Classification and mass densities of anisotropic materials

Material	**Class**	**Elastic const.**	**density** ρ (kg/m^3)
steel	isotropic	2	7850
PIC 151	transv. iso.	5	7800
spruce	orthotropic	9	430
graphite-epoxy	monoclinic	13	1600

In Section 4.1, an interpolation method for the calculation of the anisotropic fundamental solutions has been described. Since execution speed is of great importance, linear Lagrange interpolation is used. In order to get an idea of the functions that have to be interpolated, a plot of the fundamental solution ru^*_{22} and its derivative $r^3 t^*_{23,1}$ over θ_1 and θ_2 is given for all four materials in Figs. 1 and 2. It can be seen that for higher degrees of anisotropy, a finer grid is needed for an accurate

Table 2 : Elasticity matrices **C** of anisotropic materials ([C]=1 GPa)

steel (isotropic)

$$\begin{bmatrix} 282.7 & 121.2 & 121.2 & 0 & 0 & 0 \\ 121.2 & 282.7 & 121.2 & 0 & 0 & 0 \\ 121.2 & 121.2 & 282.7 & 0 & 0 & 0 \\ 0 & 0 & 0 & 80.8 & 0 & 0 \\ 0 & 0 & 0 & 0 & 80.8 & 0 \\ 0 & 0 & 0 & 0 & 0 & 80.8 \end{bmatrix}$$

PIC 151 (transversely isotropic)

$$\begin{bmatrix} 107.6 & 63.1 & 63.9 & 0 & 0 & 0 \\ 63.1 & 107.6 & 63.9 & 0 & 0 & 0 \\ 63.9 & 63.9 & 100.4 & 0 & 0 & 0 \\ 0 & 0 & 0 & 19.6 & 0 & 0 \\ 0 & 0 & 0 & 0 & 19.6 & 0 \\ 0 & 0 & 0 & 0 & 0 & 22.2 \end{bmatrix}$$

spruce (orthotropic)

$$\begin{bmatrix} 0.44 & 0.32 & 0.19 & 0 & 0 & 0 \\ 0.32 & 16.27 & 0.45 & 0 & 0 & 0 \\ 0.19 & 0.45 & 0.78 & 0 & 0 & 0 \\ 0 & 0 & 0 & 0.61 & 0 & 0 \\ 0 & 0 & 0 & 0 & 0.039 & 0 \\ 0 & 0 & 0 & 0 & 0 & 0.76 \end{bmatrix}$$

graphite-epoxy (monoclinic)

$$\begin{bmatrix} 95.5 & 28.9 & 4.03 & 0 & 0 & 44.7 \\ 28.9 & 25.9 & 4.65 & 0 & 0 & 15.6 \\ 4.03 & 4.65 & 16.3 & 0 & 0 & 0.54 \\ 0 & 0 & 0 & 4.40 & -1.78 & 0 \\ 0 & 0 & 0 & -1.78 & 6.45 & 0 \\ 44.7 & 15.6 & 0.54 & 0 & 0 & 32.7 \end{bmatrix}$$

interpolation, especially for the derivatives of the fundamental solution. The 'degree of anisotropy' is a term that is somewhat difficult to define. Within the framework of this paper, however, a higher degree of anisotropy means a higher deviation of the anisotropic results from those that are obtained using the isotropic part of the elasticity tensor. This deviation is influenced by the differences in magnitude between the elastic constants rather than by the number of independent constants (Figs. 1 and 2 show steep gradients for the strongly anisotropic materials like spruce and graphite-epoxy). This means that, e.g., a monoclinic material does not necessarily possess a higher degree of anisotropy (as defined in this paper) than a transversely isotropic material, even though this is the case for the materials used in this publication.

To assess the effect of the grid size on the accuracy of the calculations, an elastostatic analysis is performed with the model shown in Fig. 3. The sidelength of the cube is 10 mm, it is clamped at one face and subjected to a surface traction of

Table 3 : Discretizations used in the computations

Method	Elements		dofs
FEM	125	lin.	648
		quad.	2268
BEM	150	lin.	456
		quad.	1356

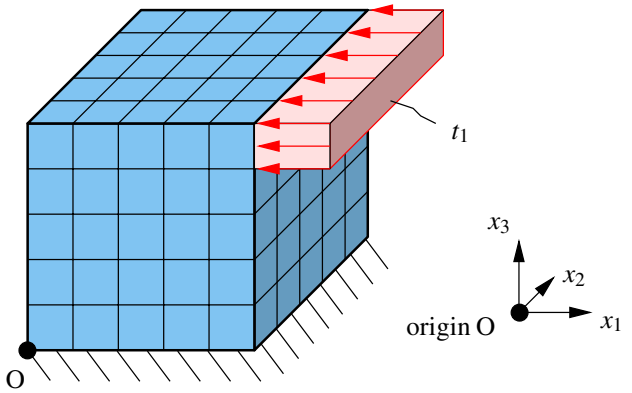

Figure 3 : Cube loaded with surface pressure $t_1 = 10$ N/mm^2

$t_1 = -10$ N/mm^2 on another. The discretization is uniform, as shown in the figure, and the methods which have been used are listed in Tab. 3.

5.2.1 *Convergence of interpolation*

Boundary Element computations have been performed for all four materials using linear and quadratic elements, with interpolation grids of size 100×100, 200×200, 400×400, and 800×800. The results are shown in Tab. 4. For the isotropic material, the results obtained using the closed form Kelvin solution are listed as a reference instead of the results obtained using the 800×800 grid. It can be observed that for increasing degree of anisotropy, a finer grid is needed for an accurate interpolation. For the materials used in this paper, it appears that a grid size of 400×400 gives sufficiently accurate results, even for the highly anisotropic materials spruce and graphite-epoxy. This is true for the displacements as well as stresses, so that in all the following calculations, a 400×400 linear Lagrange interpolation scheme is used for the approximate calculation of the fundamental solutions.

5.2.2 *Accuracy of results compared to FEM*

In order to assess the accuracy of the results obtained with the proposed Boundary Element Method, the results are compared with Finite Element computations, see Tab. 5. FE computations have also been performed on a refined mesh of 10×10×10 elements, using both linear and quadratic elements. The solutions obtained with the quadratic elements are

Table 4 : BEM computations for different grid sizes (units $[u]=10^{-4}$ mm, $[\sigma]=1$ N/mm^2)

steel (isotropic)						
	$\mathbf{u_1(10,0,10)}$		$\mathbf{\sigma_{13}(6,6,8)}$		$\mathbf{\sigma_{11}(6,6,8)}$	
grid	lin.	quad.	lin.	quad.	lin.	quad.
100×100	-7.280	-7.489	-2.302	-2.427	-3.180	-3.213
200×200	-7.297	-7.506	-2.309	-2.435	-3.179	-3.212
400×400	-7.301	-7.511	-2.312	-2.437	-3.179	-3.212
isotropic	-7.303	-7.512	-2.312	-2.438	-3.180	-3.213
PIC 151 (transversely isotropic)						
	$\mathbf{u_1(10,0,10)}$		$\mathbf{\sigma_{13}(6,6,8)}$		$\mathbf{\sigma_{11}(6,6,8)}$	
grid	lin.	quad.	lin.	quad.	lin.	quad.
100×100	-27.90	-28.73	-2.286	-2.400	-3.200	-3.227
200×200	-27.98	-28.81	-2.295	-2.409	-3.199	-3.226
400×400	-28.00	-28.83	-2.298	-2.412	-3.199	-3.226
800×800	-28.00	-28.83	-2.298	-2.412	-3.199	-3.226
spruce (orthotropic)						
	$\mathbf{u_1(10,0,10)}$		$\mathbf{\sigma_{13}(6,6,8)}$		$\mathbf{\sigma_{11}(6,6,8)}$	
grid	lin.	quad.	lin.	quad.	lin.	quad.
100×100	-6789	-7189	-2.100	-2.465	-2.996	-3.010
200×200	-6830	-7233	-2.121	-2.489	-3.009	-3.023
400×400	-6841	-7244	-2.126	-2.495	-3.017	-3.032
800×800	-6843	-7247	-2.128	-2.497	-3.014	-3.028
graphite-epoxy (monoclinic)						
	$\mathbf{u_1(10,0,10)}$		$\mathbf{\sigma_{13}(6,6,8)}$		$\mathbf{\sigma_{11}(6,6,8)}$	
grid	lin.	quad.	lin.	quad.	lin.	quad.
100×100	-92.41	-97.23	-2.153	-2.403	-2.842	-2.829
200×200	-92.93	-97.79	-2.170	-2.419	-3.004	-3.004
400×400	-93.06	-97.93	-2.176	-2.425	-2.996	-2.995
800×800	-93.09	-97.96	-2.177	-2.426	-2.993	-2.991

taken as a reference.

Regarding the displacement solution $u_1(10,0,10)$, it can be observed that the Boundary Element computations yield about the same accuracy as the Finite Element computations for all materials used in the calculations. This is the case for linear as well as for quadratic elements, although with linear elements, the BEM has a slight advantage for weakly anisotropic materials, and the FEM for strongly anisotropic materials.

Analyzing the results of the internal stress calculations, however, reveals an increased accuracy of the Boundary Element computations. Regarding first the computational results obtained using linear elements, it can be seen that independent of the degree of anisotropy of the material, the Boundary Element results are much more accurate than the Finite Element results. This is due to the fact that the Boundary Element Method is a mixed method, approximating both displacements and tractions with shape functions of the same degree, whereas in the classical Finite Element Method the stresses are calculated by derivation of the shape functions, which reduces the accuracy. The results from Tab. 5 also show that in the present example, the advantage of the BEM over the FEM with respect to stress calculations is not as evident when using quadratic elements, where it seems that the FEM yields about the same accuracy.

5.3 Anisotropic particular solution

In the Dual Reciprocity Method, the source term, which appears under the domain integral, is approximated by a series of prescribed tensor functions f_{in}^q and coefficients α_n^q (cf. Eq. 17). The functions f_{in}^q have to be chosen in such a way that a good convergence of the approximation is guaranteed. Radial basis functions (RBFs) possess this property (Powell (1992); Golberg and Chen (1994)) and are therefore often used in DRM analyses. In dynamic elasticity, the radial basis function $f_{in}^q = \delta_{in}(1+r)$ (or alternatively $f_{in}^q = \delta_{in}(C-r)$), for which closed form particular solutions exist, is often used and yields good results (Nardini and Brebbia (1982); Dominguez (1993);

Table 5 : Comparison of BEM and FEM computations (units $[u]=10^{-4}$ mm, $[\sigma]=1$ N/mm^2)

steel (isotropic)						
	$\mathbf{u_1(10,0,10)}$		$\boldsymbol{\sigma_{13}(6,6,8)}$		$\boldsymbol{\sigma_{11}(6,6,8)}$	
method	lin.	quad.	lin.	quad.	lin.	quad.
BEM	-7.301	-7.511	-2.312	-2.437	-3.179	-3.212
FEM 5×5×5	-7.148	-7.515	-1.817	-2.675	-3.009	-3.233
FEM 10×10×10	-7.414	**-7.524**	-2.264	**-2.500**	-3.152	**-3.218**
PIC 151 (transversely isotropic)						
	$\mathbf{u_1(10,0,10)}$		$\boldsymbol{\sigma_{13}(6,6,8)}$		$\boldsymbol{\sigma_{11}(6,6,8)}$	
method	lin.	quad.	lin.	quad.	lin.	quad.
BEM	-28.00	-28.83	-2.298	-2.412	-3.199	-3.226
FEM 5×5×5	-26.90	-28.80	-1.828	-2.634	-2.944	-3.278
FEM 10×10×10	-28.29	**-28.88**	-2.246	**-2.471**	-3.137	**-3.239**
spruce (orthotropic)						
	$\mathbf{u_1(10,0,10)}$		$\boldsymbol{\sigma_{13}(6,6,8)}$		$\boldsymbol{\sigma_{11}(6,6,8)}$	
method	lin.	quad.	lin.	quad.	lin.	quad.
BEM	-6841	-7244	-2.126	-2.495	-3.017	-3.032
FEM 5×5×5	-7024	-7218	-1.959	-2.671	-2.932	-3.015
FEM 10×10×10	-7160	**-7264**	-2.319	**-2.535**	-2.992	**-3.021**
graphite-epoxy (monoclinic)						
	$\mathbf{u_1(10,0,10)}$		$\boldsymbol{\sigma_{13}(6,6,8)}$		$\boldsymbol{\sigma_{11}(6,6,8)}$	
method	lin.	quad.	lin.	quad.	lin.	quad.
BEM	-93.06	-97.93	-2.176	-2.425	-2.996	-2.995
FEM 5×5×5	-94.71	-97.87	-1.767	-2.641	-2.813	-3.063
FEM 10×10×10	-96.84	**-97.77**	-2.220	**-2.514**	-3.066	**-3.088**

Table 6 : Results obtained with different approximation functions f_{in}^q (units $[u]=1$ μm, $[t]=1$ N/mm^2)

f_{in}	$\boldsymbol{\delta_{im}(1+r)}$		**Eqn** (41)		exact
internal nodes	**0**	**19**	**0**	**19**	—
$\mathbf{u_1(100,5,5)}$	24.993	25.014	24.981	24.997	25.000
$\mathbf{u_1(x_1=100)}$ (max. error in %)	0.07	0.06	0.11	0.05	—
$\mathbf{t_1(0,5,5)}$	-100.086	-100.172	-99.992	-100.059	-100.000
$\mathbf{t_1(x_1=0)}$ (max. error in %)	0.20	0.17	0.17	0.11	—

Agnantiaris, Polyzos, and Beskos (1998)).

For anisotropic elasticity, as already mentioned, it is not possible to obtain a particular solution in closed form. Hence the approach described in Section 4.3 is used in this paper, where the particular solution u_{kn}^q is prescribed (cf. Eq. 41), and the approximation function f_{in}^q is calculated from Eq. 44. It is difficult, however, to make any statements about the convergence of this function f_{in}^q. Therefore, in order to assess the accuracy of the results obtained with this approach, they are compared with the results obtained by using the $1+r$ function, for which the convergence is known. As a model, a prismatic rod with Young's modulus $E = 200\,000$ N/mm^2 and Poisson's ratio $\nu = 0$ is used. It is clamped at one end and subjected to a constant body force $b = 1$ N/mm^3 in x_1-direction as shown in Fig. 4.

The analytical solution and numerical results are given in Tab. 6. It can be observed that for this example, the particular solution proposed in Eq. 41 yields excellent results for the displacements u_1 at the free end and tractions t_1 at the clamped end. These results, which are even slightly better than the results obtained with the 'classical' $1+r$ function, support the choice of Eq. 41 as particular solution.

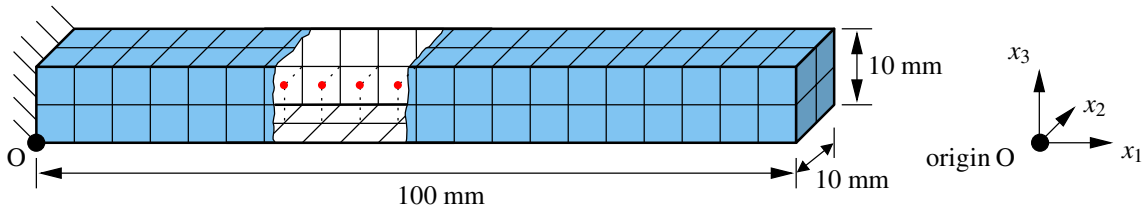

Figure 4 : Rod discretization with 19 equally spaced internal nodes

Table 7 : Discretizations and methods used in the forced vibration calculations

Method	Elements		dofs
FEM	350	lin.	1728
		quad.	6228
BEM	375	lin.	1353
		quad.	3453

6 Dynamic analysis

6.1 Forced vibrations

In forced vibration analysis, harmonic time dependence

$$\psi(x_i,t) = \hat{\psi}(x_i)\sin\omega t \tag{45}$$

with angular frequency ω and amplitude $\hat{\psi}$ is assumed for all field quantities ψ. The system of equations Eq. 25 obtained with the proposed Dual Reciprocity Boundary Element Method then becomes

$$\left(\boldsymbol{H} - \omega^2 \boldsymbol{M}\right)\check{\boldsymbol{u}} = \boldsymbol{G}\check{\boldsymbol{t}}\,, \tag{46}$$

where body forces have been neglected. In Eq. 46, the vectors $\check{\boldsymbol{u}}$ and $\check{\boldsymbol{t}}$ now contain the nodal amplitudes of displacements and tractions; the symbol $\hat{(\cdot)}$ has been omitted for clarity. Solution of the linear system of equations given in Eq. 46 does not pose any problems, since the time dependence of the field variables has been eliminated by the time harmonic formulation.

The model of the investigated body is shown in Fig. 5, along with the discretization. The numerical methods used for the calculations are given in Tab. 7, where it has to be noted that 99 internal nodes have been used for both the linear and quadratic BEM calculations. The vibrations are excited by a time-harmonic surface traction $\bar{t}_1 = -100$ N/mm^2 for steel, PIC 151, and graphite-epoxy, and $\bar{t}_1 = -1$ N/mm^2 for spruce. The angular frequency ω is chosen as 100 kHz for steel, 50 kHz for PIC 151, 20 kHz for spruce, and 50 kHz for graphite-epoxy. All these frequencies lie around the 7th eigenfrequency of the respective problem.

The deformations are shown in Fig. 6 for the different materials, with the contour plot giving the displacement u_1. In

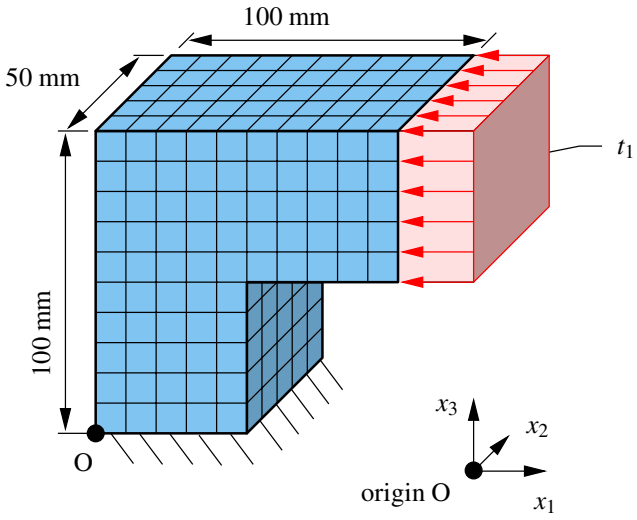

Figure 5 : Model used in dynamic analysis; the prescribed tractions are $t_1 = \bar{t}_1 \sin\omega t$ for forced vibrations, and $t_1 = \bar{t}_1\, H(t)$ for transient analysis

order to assess the accuracy of the methods, the displacement $u_1(50,0,x_3)$ and stress $\sigma_{11}(37.5,12.5,x_3)$ are shown in Figs. 7-10. Excellent agreement between the FEM and BEM displacement results can be observed for all materials, for both linear and quadratic element shape functions. The stress computations of the quadratic FEM and BEM, too, show excellent agreement. As expected, the linear BEM results are more accurate than the FEM results, especially for the weakly anisotropic materials steel and PIC 151. For graphite-epoxy, the agreement between the FEM and BEM stress results is satisfactory, albeit not as good as in the other calculations.

6.2 Transient analysis

For transient analysis, the model shown in Fig. 5 is used again, but now instead of the time-harmonic excitation, a Heaviside-type surface traction with $\bar{t}_1 = -0.1$ N/mm^2 is applied on the specified face. This load case is usually a very effective test for the performance of a numerical method, since the Heaviside function contains the complete spectrum of frequencies.

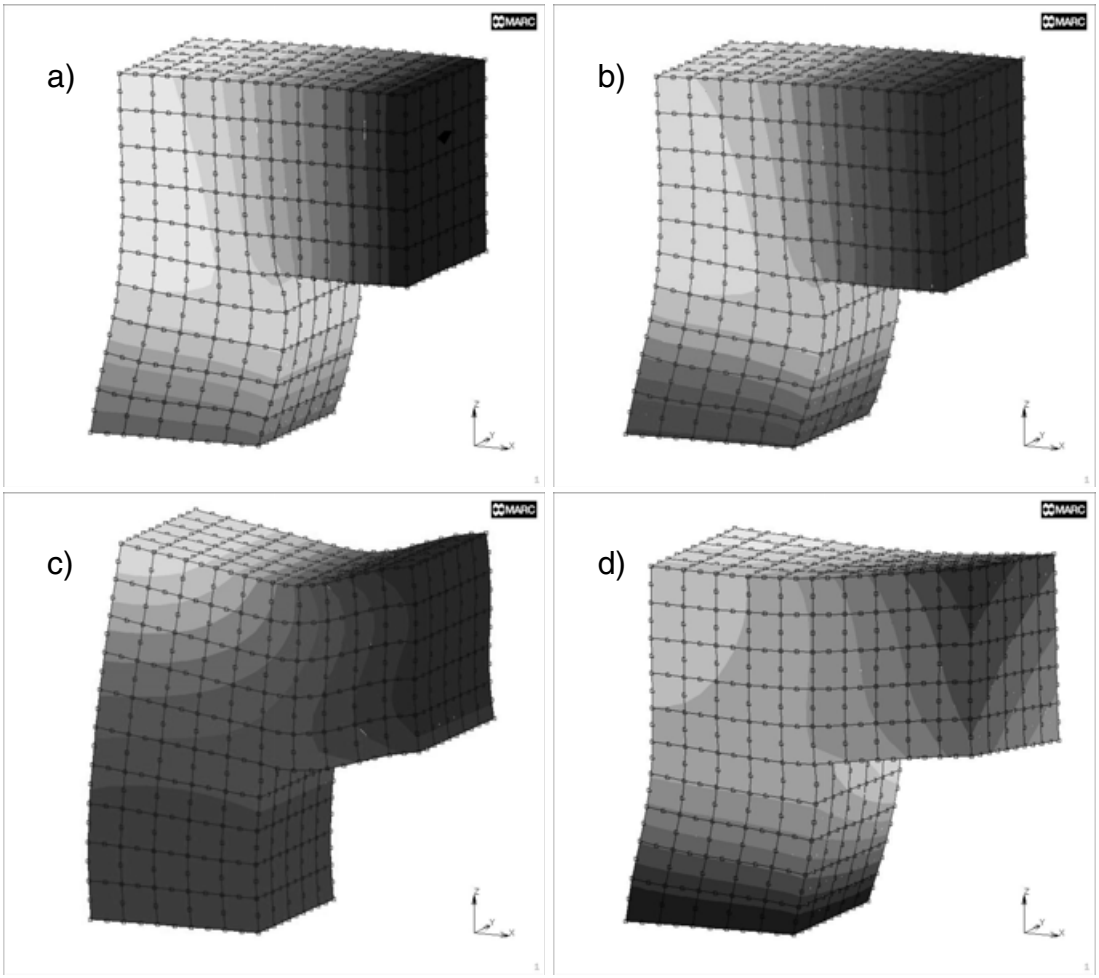

Figure 6 : Forced vibration analysis: deformed shapes for a) steel ($\omega = 100$ kHz), b) PIC 151 ($\omega = 50$ kHz), c) spruce ($\omega = 20$ kHz), d) graphite-epoxy ($\omega = 50$ kHz)

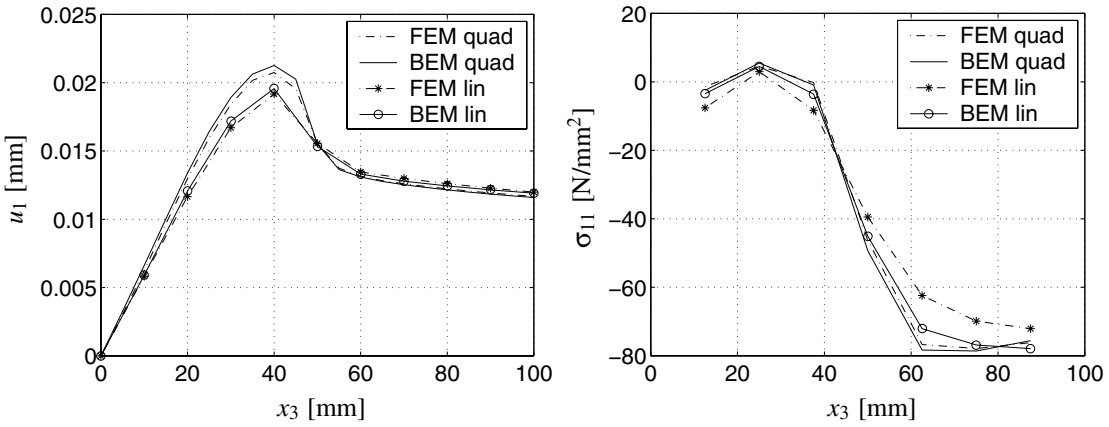

Figure 7 : Forced vibration analysis: displacement $u_1(50, 0, x_3)$ and stress $\sigma_{11}(37.5, 12.5, x_3)$ for isotropic steel

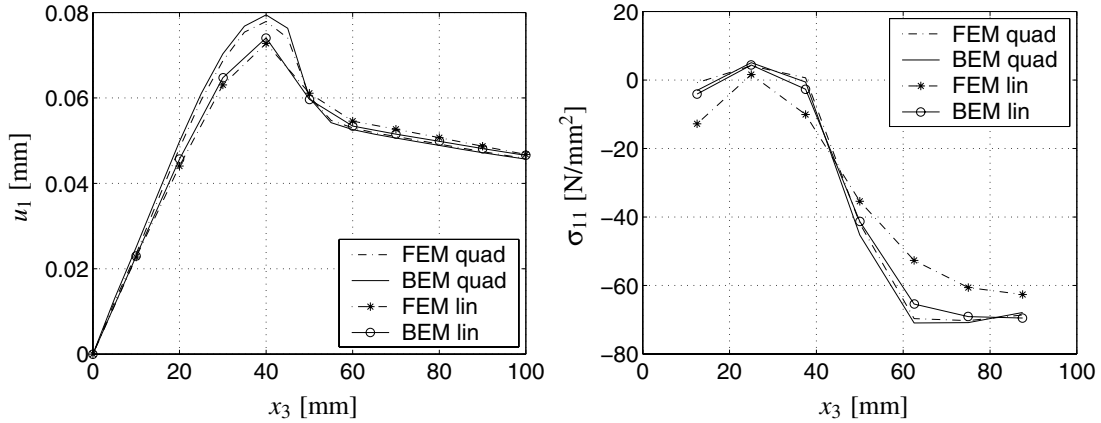

Figure 8 : Forced vibration analysis: displacement $u_1(50,0,x_3)$ and stress $\sigma_{11}(37.5,12.5,x_3)$ for PIC 151

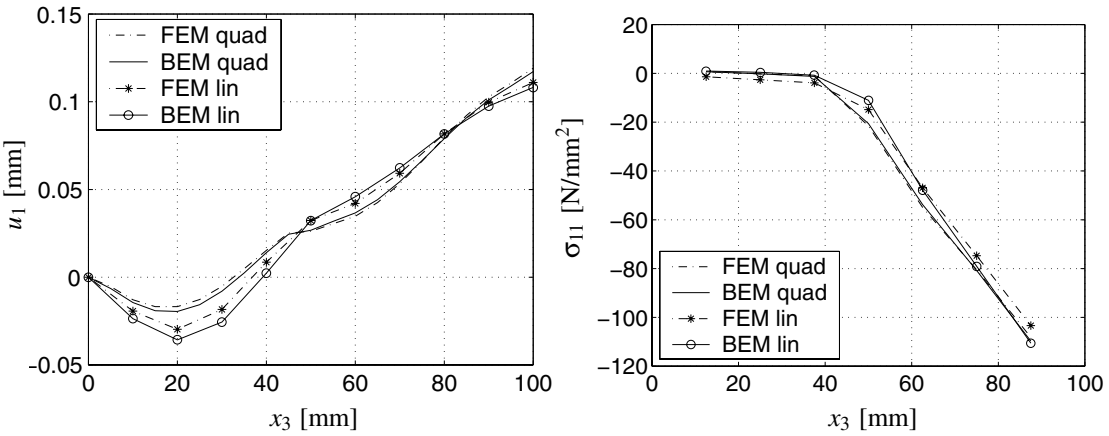

Figure 9 : Forced vibration analysis: displacement $u_1(50,0,x_3)$ and stress $\sigma_{11}(37.5,12.5,x_3)$ for spruce

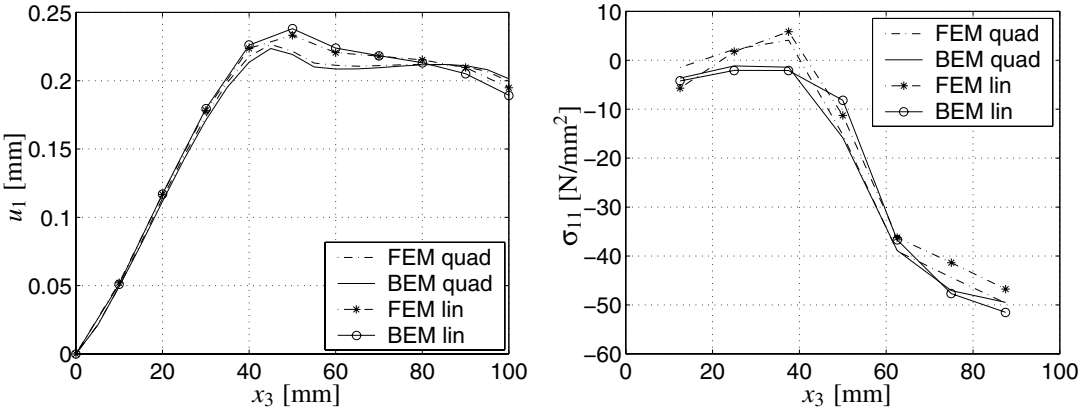

Figure 10 : Forced vibration analysis: displacement $u_1(50,0,x_3)$ and stress $\sigma_{11}(37.5,12.5,x_3)$ for graphite-epoxy

It has already been mentioned that the system matrices obtained in the DR-BEM are non-symmetric. This leads to complex eigenvalues, which can cause divergence in the time integration. However, as already observed by Nardini and Brebbia (1985), the complex eigenfrequencies usually appear in the higher modes, which are not needed in the analysis anyway since they yield inaccurate results due to the finite discretization of the continuum. Therefore, in order to obtain re-

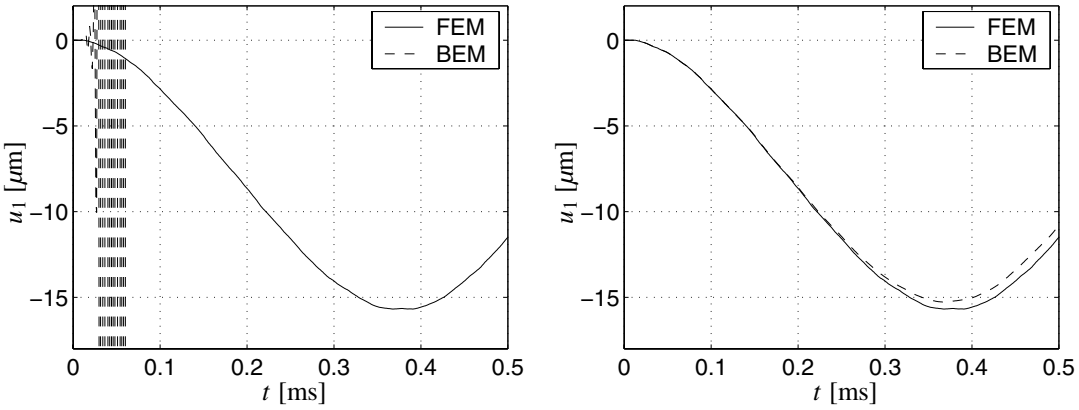

Figure 11 : Time histories of displacement $u_1(0,0,100;t)$ for graphite-epoxy, calculated with 99 internal nodes using Newmark's algorithm (left) and Houbolt's algorithm (right)

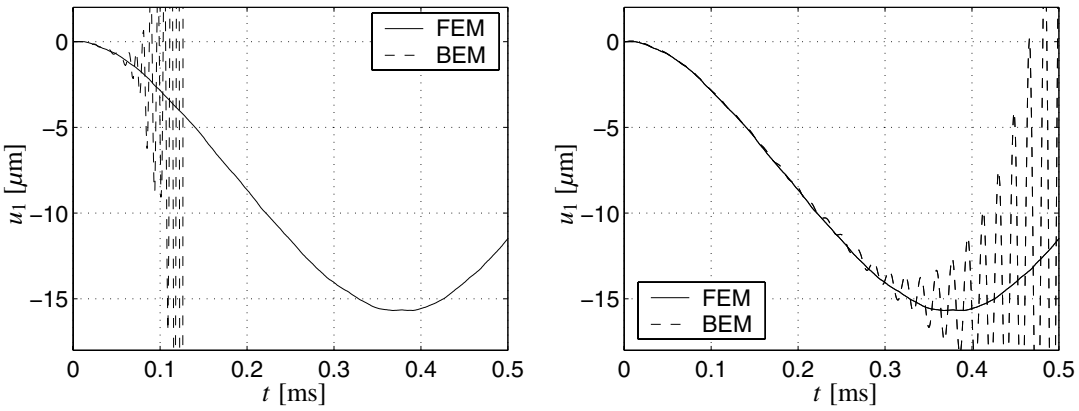

Figure 12 : Time histories of displacement $u_1(0,0,100;t)$ for graphite-epoxy, calculated with 3 internal nodes using Houbolt's algorithm with direct integration (left) and modal superposition using the first 100 nodes (right)

liable and accurate results, the time-integration scheme has to be chosen in such a way as to eliminate or damp the higher frequencies.

In Figs. 11 and 12 some factors which influence the divergence in the time integration are shown. The time step size is chosen as $\Delta t = 1\ \mu$s, hence the figures contain 500 time steps. Fig. 11 demonstrates the influence of the time stepping scheme when 99 internal nodes are used. In the left graph, the standard Newmark algorithm with $\delta = 0.5$ and $\alpha = 0.25$ is applied (Newmark (1959)), and the results start diverging after few time steps. On the right, Houbolt's algorithm is employed (Houbolt (1950)), and the integration remains stable. This is because the algorithm provides numerical damping, particularly at the higher frequencies, which are the complex ones causing problems in the DR-BEM analysis.

In Fig. 12, the same problem is solved, but this time with only three internal nodes and hence a less accurate mass matrix. One can see that now the numerical damping introduced by Houbolt's algorithm is no longer sufficient and the results diverge rapidly. The performance can be improved by using the modal superposition method, employing only the first 100 modes, but the results are still not satisfying.

Thus, from these calculations, the following conclusions can be drawn:

- increasing the number of internal nodes improves the approximation of the domain term and yields a more accurate mass matrix;
- employing a time stepping scheme that displays numerical damping helps in suppressing the deleterious modes resulting from the complex eigenvalues;
- using a modal superposition approach and employing only the lower frequency modes also improves the accuracy of the results, since the complex eigenfrequencies usually appear in the higher modes.

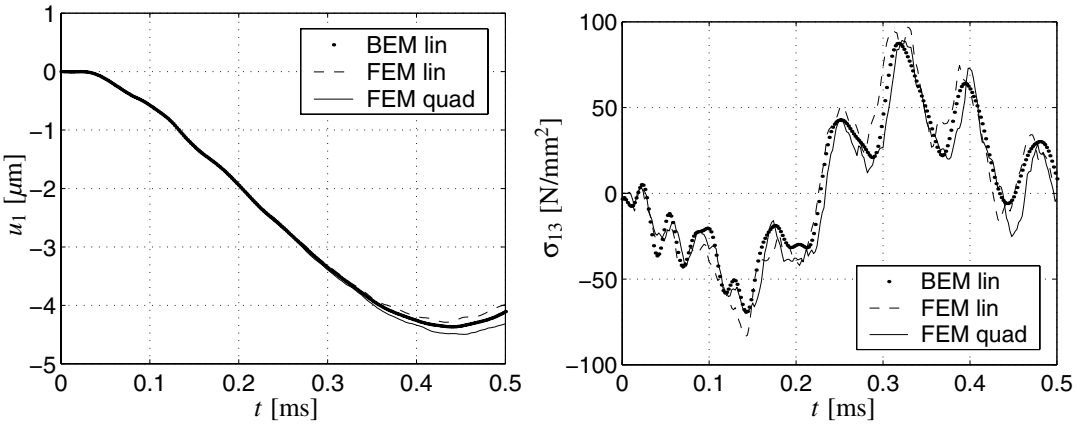

Figure 13 : Time histories of displacement $u_1(0,0,100;t)$ (left) and stress $\sigma_{13}(62.5,12.5,62.5;t)$ (right) for PIC 151; comparison of FEM (Newmark) and BEM (Newmark, $\delta = 0.7$, $\alpha = 0.5$, modal superposition using first 100 modes)

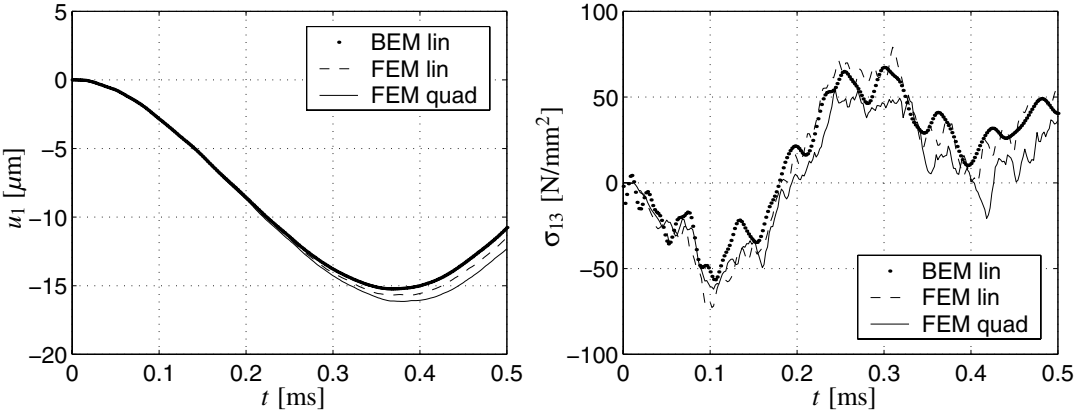

Figure 14 : Time histories of displacement $u_1(0,0,100;t)$ (left) and stress $\sigma_{13}(62.5,12.5,62.5;t)$ (right) for graphite-epoxy; comparison of FEM (Newmark) and BEM (Newmark, $\delta = 0.7$, $\alpha = 0.5$, modal superposition using first 100 modes)

Now, the transient results obtained with the present Boundary Element Method are compared to Finite Element calculations. In order to achieve a stable time-integration, modal superposition is used in the BEM calculations, employing a damped Newmark algorithm and making use of the first 100 modes only. The Finite Element results are calculated using a standard Newmark scheme. The results obtained for the displacements $u_1(0,0,100)$ and stresses $\sigma_{13}(62.5,12.5,62.5)$ are shown in Fig. 13 for PIC 151 and in Fig. 14 for graphite-epoxy. It is observed that for the transversely isotropic material, the displacements obtained with linear boundary elements are slightly better than the FE results, and for the monoclinic material, the FE results are somewhat more accurate. In case of the stresses, it is hard to make any statements about the accuracy due to the oscillations shown in the results, but the agreement is generally good.

7 Conclusions

A Boundary Element Method for the solution of three-dimensional problems of anisotropic elastodynamics has been developed. Because the use of the anisotropic dynamic fundamental solution would cause many problems and disadvantages, the present approach uses the static fundamental solution. The domain integral that appears in the representation formula is transformed to the boundary by the Dual Reciprocity Method. The resulting system of differential equations is similar to the one obtained in Finite Element analysis. Therefore, the calculation of dynamic problems such as free vibrations, time- and frequency domain analysis, can be carried out in a comparable manner, which is a great advantage over BE approaches using frequency- and time-domain fundamental solutions.

By means of numerical examples, some general questions

about the implementation have been investigated. These concern the grid size needed for the interpolation of the fundamental solutions, and the validation of the choice of the particular solution used in the approximation of the domain term. The method has then been applied to the solution of a three-dimensional forced vibration problem using various materials with different degrees of anisotropy. The results show excellent agreement between the new method and Finite Element computations for the displacements. With regard to the stress calculation, it was shown that the results obtained by using linear boundary elements are more accurate than those obtained with linear finite elements. Also, a transient analysis has been performed, where the numerical problems resulting from the non-symmetric matrices were demonstrated. Some propositions for their solution have been described briefly, and it was shown that excellent results are obtained when using appropriate solution schemes.

It can therefore be stated that the suggested method presents an excellent alternative to FEM for the solution of problems of anisotropic elastodynamics, especially for stress calculations.

Acknowledgement: Support by the Deutsche Forschungsgemeinschaft (DFG) of the Graduate Collegium 'Modelling and discretization methods for continua and fluids' (GKKS) at the University of Stuttgart is gratefully acknowledged.

References

Agnantiaris, J. P.; Polyzos, D.; Beskos, D. E. (1998): Three-dimensional structural vibration analysis by the dual reciprocity BEM. *Computational Mechanics*, vol. 21, pp. 372–381.

Ahmad, S.; Banerjee, P. K. (1986): Free vibration analysis by BEM using particular integrals. *Journal of Engineering Mechanics ASCE*, vol. 112, no. 7, pp. 682–695.

Atkinson, K. E. (1985): The numerical evaluation of particular solutions for Poisson's equation. *IMA Journal of Numerical Analysis*, vol. 5, pp. 319–338.

Bacon, D. J.; Barnett, D. M.; Scattergood, R. O. (1980): *Progress in materials science*, volume 23, chapter 2: Anisotropic continuum theory of lattice defects, pp. 51–262. Pergamon Press, Oxford, 1980.

Banerjee, P. K. (1994): *The boundary element methods in engineering*. McGraw-Hill, London, second edition.

Barnett, D. M. (1972): The precise evaluation of derivatives of the anisotropic elastic Green's functions. *phys. stat. sol. (b)*, vol. 49, pp. 741–748.

Brebbia, C.; Telles, J.; Wrobel, L. (1984): *Boundary element techniques*. Springer-Verlag, Berlin.

Deb, A. (1991): *Advanced development of the BEM for linear and nonlinear analyses of anisotropic solids*. PhD thesis, Buffalo State University, 1991.

Dederichs, P. H.; Leibfried, G. (1969): Elastic Green's function for anisotropic cubic crystals. *Phys. Rev.*, vol. 188, no. 3, pp. 1175–1183.

Ding, H.; Liang, J.; Chen, B. (1997): The united point force solution for both isotropic and transversely isotropic media. *Communications in Numerical Methods in Engineering*, vol. 13, no. 2, pp. 95–102.

Dominguez, J. (1993): *Boundary elements in dynamics*. Computational Mechanics Publications, Southampton.

Gaul, L.; Fiedler, C. (1996): *Boundary Element Methods in Statics and Dynamics (in German)*. Verlag Vieweg, Braunschweig.

Gel'fand, I. M.; Graev, M. I.; Vilenkin, N. Y. (1966): *Generalized functions*, volume 5: Integral geometry and representation theory. Academic Press, New York.

Golberg, M. A. (1995): The numerical evaluation of particular solutions in the BEM - a review. *Boundary Element Communications*, vol. 6, pp. 99–106.

Golberg, M. A.; Chen, C. S. (1994): The theory of radial basis functions applied to the BEM for inhomogeneous partial differential equations. *Boundary Element Communications*, vol. 5, pp. 57–61.

Gründemann, H. (1989): A general procedure transferring domain integrals onto boundary integrals in BEM. *Engineering Analysis with Boundary Elements*, vol. 6, no. 4, pp. 214–222.

Houbolt, J. C. (1950): A recurrence matrix solution for the dynamic response of elastic aircraft. *J. Aeronautical Sciences*, vol. 17, pp. 540–550.

Nardini, D.; Brebbia, C. A. (1982): A new approach to free vibration analysis using boundary elements. In *Boundary element methods in engineering*, pp. 312–326, Berlin. Springer-Verlag.

Nardini, D.; Brebbia, C. A. (1985): *Topics in boundary element research*, volume 2: Time-dependent and vibration problems, chapter 7: Boundary integral formulation of mass matrices for dynamic analysis, pp. 191–208. Springer-Verlag, Berlin, 1985.

Nardini, D.; Brebbia, C. A. (1986): Transient boundary element elastodynamics using the dual reciprocity method and modal superposition. In *Boundary elements VIII*, pp. 435–443, Berlin. Springer-Verlag.

Newmark, N. M. (1959): A method of computation for structural dynamics. *ASCE. Journal of the Engineering Mechanics Division*, vol. 85, pp. 67–94.

Pan, Y. C.; Chou, T. W. (1976): Point force solution for an infinite transversely isotropic solid. *J. Appl. Mech.*, vol. 43, no. 4, pp. 608–612.

Polyzos, D.; Dassios, G.; Beskos, D. E. (1994): On the equivalence of dual reciprocity and particular integral approaches in the BEM. *Boundary Element Communications*, vol. 5, pp. 285–288.

Powell, M. J. D. (1992): *Advances in numerical analysis*, volume II, chapter 3: The theory of radial basis function approximation in 1990, pp. 105–210. Oxford Science Publ., Oxford, 1992.

Schclar, N. A. (1994): *Anisotropic analysis using boundary elements*. Computational Mechanics Publications.

Vogel, S. M.; Rizzo, F. J. (1973): An integral equation formulation of three dimensional anisotropic elastostatic boundary value problems. *J. Elasticity*, vol. 3, no. 3, pp. 203–216.

Wang, C.-Y.; Achenbach, J. D. (1993): A new method to obtain 3-D Green's functions for anisotropic solids. *Wave Motion*, vol. 18, pp. 273–289.

Wang, C.-Y.; Achenbach, J. D. (1994): Elastodynamic fundamental solutions for anisotropic solids. *Geophys. J. Int.*, vol. 118, pp. 384–392.

Wang, C.-Y.; Achenbach, J. D. (1995): Three-dimensional time-harmonic elastodynamic Green's functions for anisotropic solids. *Proc. Royal Soc. London A*, vol. 449, pp. 441–458.

Wang, C. Y.; Achenbach, J. D.; Hirose, S. (1996): Two-dimensional time domain BEM for scattering of elastic waves in solids of general anisotropy. *Int. J. Solids Structures*, vol. 33, no. 26, pp. 3843–3864.

Wilson, R. B.; Cruse, T. A. (1978): Efficient implementation of anisotropic three dimensional boundary-integral equation stress analysis. *Int. J. Numer. Meth. Engng.*, vol. 12, pp. 1383–1397.

Zheng, T.; Dravinski, M. (2000): Scattering of elastic waves by a 3D anisotropic basin. *Earthquake Engng. Struct. Dyn.*, vol. 29, pp. 419–439.